Nanoscale Advances

ROYAL SOCIETY OF CHEMISTRY

PAPER

View Article Online
View Journal | View Issue



Cite this: *Nanoscale Adv.*, 2022, **4**, 4756

# A wireless "Janus" soft gripper with multiple tactile sensors†

Lei Han, *[a] Rui Wang, [a] Yupeng Dong,[a] Xun Zhang,[a] Chenggen Wu[a] and Xiaoguang Zhao[b]

Biomimetic properties allow soft robots to complexly interact with the environment. As the bridge between the robot and the operating object, the gripping hand is an important organ for its connection with the outside world, which requires the ability to provide feedback from the grasped object, similar to the human sensory and nervous system. In this work, to cope with the difficulty of integrating complex sensing and communication systems into flexible soft grippers, we propose a GO/PI composite bilayer film-based gripper with two types of tactile sensors and a LC passive wireless transmission module to obtain the grip information and transmit it to the processor. The bilayer film structure demonstrates good photothermal driving performance. Pressure and material sensors are located at the tips of the gripper's fingers to acquire tactile information which is wirelessly transmitted to the processor for analysis *via* the LC circuit. The grasping and feedback of the gripper are presented through an intelligent display system, realizing the wireless interconnection between the robot terminal and processing system, exhibiting broad application potential.

Received 2nd April 2022
Accepted 4th October 2022

DOI: 10.1039/d2na00208f

rsc.li/nanoscale-advances



## Introduction

Biological systems can perform complex tasks with high compliance levels, which makes them a great source of inspiration for soft robotics.[1–9] For creatures, including both animals and plants, grasping and manipulation are fundamental ways to interact with the environment. Many animals and plants usually take advantage of their bodies, such as human hands, eagle claws, elephant trunks, flytrap tentacles, and sundew tendrils as end effectors to collect sensory information such as pressure and strain to complete many interaction-based tasks, including hunting, nesting, and feeding. Compared with rigid robots, biomimetic soft robots have a high degree of deformability and dexterity. "Janus" soft robots based on a flexible bilayer film structure can grasp and manipulate various types of objects.[10–12] The soft grippers convert the bilayer film structure which is mismatched caused by external environmental stimuli such as humidity,[13] electricity,[14] magnetism,[15] heat,[16] light,[17] air pressure,[18] hydraulic pressure,[19] solvent,[20] *etc.* into the mechanical movement. Electrical response, magnetic response, photo-thermal response, and multi-stimulus response grippers are commonly utilized. Although electrical response grippers have the advantages of simple operation and excellent controllability, it is necessary to connect the grippers and the power supply through a wire, which is not conducive to the application of wireless detection.[21–23] Magnetic response grippers are accompanied by high controllability due to their remote non-contact control *via* manipulating the direction and intensity of the magnetic field.[15] However, they require complex and bulky external apparatus to control the magnetic field and its gradient precisely, and as the distance from the magnetic source increases, the magnetic field strength decreases significantly. Light is considered to be one of the most promising stimuli for biomimetic soft grippers. Their non-contact drive enables the selective and precise control of the grippers through wavelength and intensity selection.[24] Photo-response grippers enable high-resolution temporal and spatial control. Various materials have been adopted in photo-responsive grippers that are triggered directly (photo-chemical)[9,25–27] or indirectly (photo-thermal)[28–34] by responding to different wavelengths from ultraviolet (UV) to near-infrared (NIR), which indicates that the photo-thermal response gripper based on the soft bilayer film has broad research prospects.

The structure design, preparation, and application of novel materials and grasping movements of the flexible gripper have been extensively studied. Few studies focus on multi-tactile sensing between the gripper and the operating object and there is also a lack of research on the transmission and interaction of tactile sensing information. Relevant tactile sensing research studies mostly concentrate on the direction of large and rigid bionic grippers.[35] Due to the size of the large-scale bionic gripper, the driving method is generally electric drive,

[a]*Key Laboratory of MEMS of the Ministry of Education, Southeast University, Nanjing, 210096, China. E-mail: hanlei@seu.edu.cn*

[b]*Department of Precision Instruments, Tsinghua University, Beijing, 100084, China*

† Electronic supplementary information (ESI) available. See https://doi.org/10.1039/d2na00208f

and the detection method is usually wired sensing measurement, which limits its application in confined spaces and harsh environments.

In this article, we propose an integration of an intelligent flexible gripper with two types of tactile sensors and a LC passive wireless circuit to obtain and transmit tactile information. The grasping movements of the proposed gripper are realized by a graphene oxide/polyimide (GO/PI) composite bilayer film. Due to the difference in thermal expansion coefficients of GO and PI, the bilayer film bends toward the GO side under infrared light (IR) irradiation to achieve grasping. The tactile sensors located at the fingertips can realize the accurate measurement of the grasping force and the precise identification of the target object materials. In addition, the gripper can also communicate with the processor to realize the intelligent integrated display of tactile sensor information.

## Results and discussion

As shown in Fig. 1a, creatures manipulate objects by the grasping movement of muscles and the tactile sensation of neurons. Due to the analogous flexibility to living organisms, soft grippers can be used as a way to achieve this biological movement. Fig. 1b shows the basic composition of the grasping hand, the structure of which is similar to that of a cruciform. Graphene oxide (GO), a derivative of a two-dimensional graphene material with excellent properties, is used as the host material so that the GO film and the PI film form a composite. The bilayer film is excited by IR to bend the four fingers for grasping the small ball located in the central area of the gripper. GO has a negative coefficient of thermal expansion (CTE) and a high coefficient of hygroscopic expansion (CHE) which is a good candidate material for the fabrication of the gripper. On

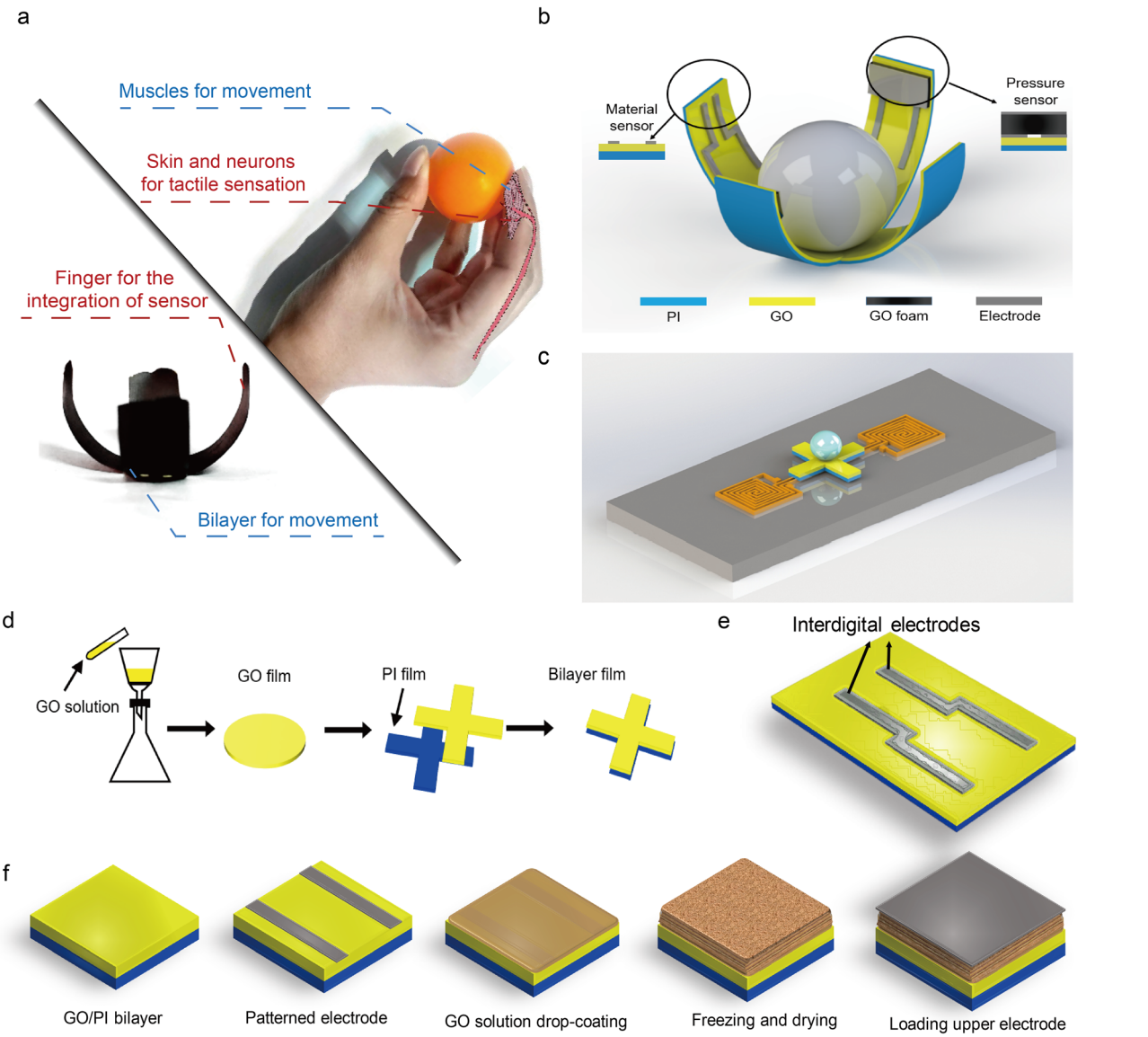


Fig. 1 Fabrication and structure of the gripper. (a) Comparison of robot and manual gripping. (b) Schematic diagram of the gripper; (c) gripper system; (d) flow chart of the preparation of GO/PI composite bilayers; (e) structure of the material sensor; (f) fabrication process of the pressure sensor.

the other hand, PI has a highly positive CTE and an ignorable CHE. Hence, the GO/PI bilayer film structure is suitable for fabricating the gripper with large bending actuation when the temperature increases, as illustrated in Note S1.† In addition, graphene and its carbon-based materials show good absorption in the wavelength range from UV to NIR. When the flexible gripper is excited by IR, due to the difference in thermal expansion coefficients of GO and PI, the gripper based on the GO/PI bilayer film bends towards the GO film side to realize the grasping movement of the gripper.

A pair of sensors with interdigital capacitance is used to distinguish different materials, and the other pair of sensors is made of a sandwich structure to detect pressure, where the inter-dielectric layer is a three-dimensional porous structure GO foam with good dielectric properties. Two pairs of sensors are symmetrically distributed on the finger tips of the cruciform gripper, as shown in the inset of Fig. 1b. The description of the electrode structure and dimensions is provided in Note S4.† Fig. 1c shows the structure of the entire gripper system. Two parallel-connected sandwich-structured sensitive capacitors are connected in parallel with a planar spiral inductor on the PCB to form an LC circuit. When the gripper robot grasps objects, the distance between the upper and lower electrodes decreases due to the pressure, which makes the capacitance value larger, and leads to a shift in the resonant frequency of the LC circuit that indicates the pressure value. The details of capacitive sensing are given in Note S2.† In the same way, the two interdigitated sensitive capacitors are connected in parallel with another planar spiral inductor on the PCB to form another LC circuit. When the gripper robot grasps objects of different materials, a corresponding change in the relative dielectric constant varies the interdigital capacitor, which is reflected in the resonant frequency (Note S3†).

Fig. 1d shows the fabrication process of the GO/PI composite bilayer film. The GO film is prepared by vacuum filtration, then completely peeled off from the filter paper and cut by irradiating the GO film with a focused high-power density laser beam to form the corresponding pattern. Next, the adhesive PI film (purchased from RICROWN TECHNOLOGY) is bonded to the patterned GO film, resulting in a GO/PI composite bilayer film. The interdigital electrodes for the material sensor are directly fabricated on the GO film side of the GO/PI bilayer film as shown in Fig. 1e. It consists of one group of interdigital structures and causes the initial capacitance that varies with the test material. Fig. 1f is a schematic diagram of the preparation process of the GO-based pressure sensor. First, patterned electrodes are realized on the GO film side of the prepared GO/PI bilayer film. Then, the preparation of the foam dielectric layer includes drop-coating a high-concentration GO solution on the electrodes, freezing and vacuum drying. Finally, the upper electrode structure of the pressure sensor is prepared on the GO foam, and the overall structure is assembled.

### Structural and material characterization

As shown in Fig. 2, the gripper robot is characterized. Fig. 2a shows the optical and scanning electron microscopy (SEM)

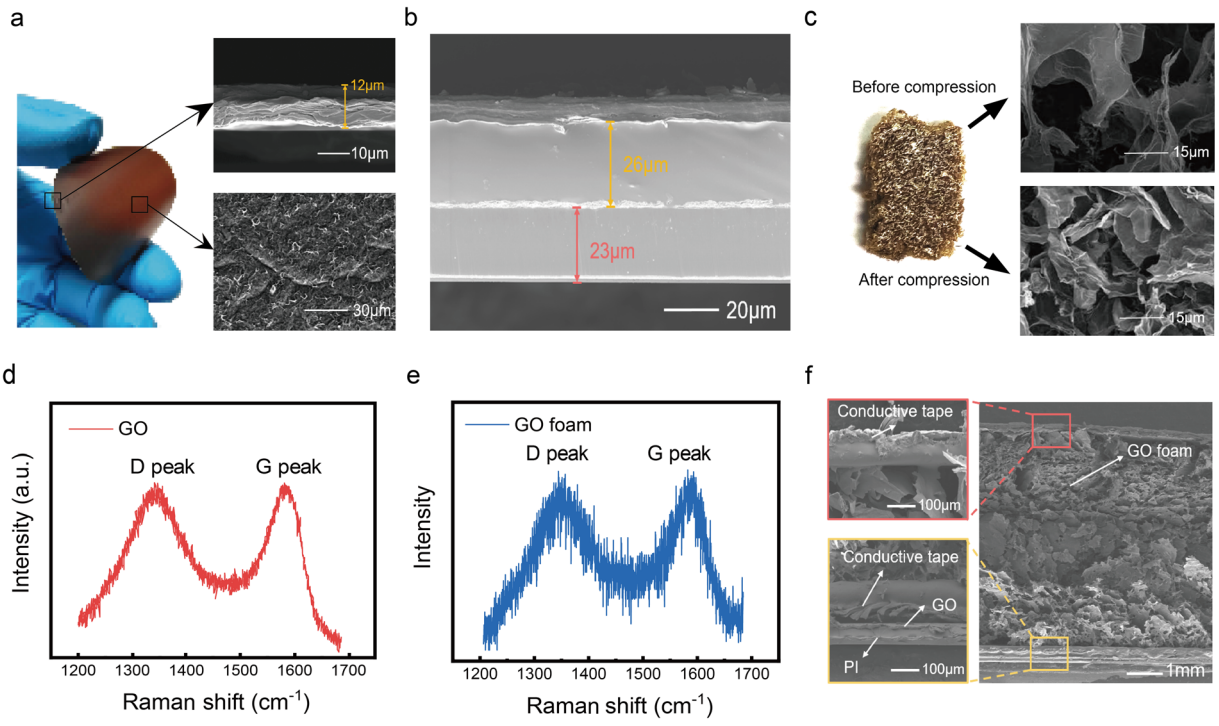


Fig. 2 Structure characterization of the gripper. (a) Optical (left) and SEM image of the cross-section (upper right) and surface (bottom right) for pristine GO; (b) SEM image of the cross-section for the GO/PI composite bilayer film, red: PI, orange: adhesive; (c) SEM images of GO foam before (upper) and after (bottom) compression; (d) Raman spectra of the GO film. (e) Raman spectra of GO foam. (f) Structural cross-section SEM of the sandwich structure pressure sensor.

image of the GO film, the cross-section of which indicates that the GO film with a thickness of 12 μm has an obvious layered structure. The top-down SEM image shows that the GO surface is flat with only some slight wrinkles observed. AFM characterization of the surface of the GO film is additionally performed (Note S5 and Fig. S7†), from which it can be confirmed that the surface of the GO film is relatively flat and has no effect on the performance of the gripper. Fig. 2b shows the SEM image of the cross-section of the GO/PI composite bilayer film. The gap between the GO film and the PI film is negligible, and the thickness of the GO and the PI film is about 10 μm and 60 μm, respectively.

Fig. 2c shows the optical and SEM image of the GO foam which exhibits an ultra-light three-dimensional porous structure, which is formed because the GO sheets are squeezed by the continuously generated ice crystals during the freezing process and crosslinked with each other under the intermolecular forces. After sublimation of the ice crystal, the remaining space is filled with air. The size of air holes and the density of GO foam can be adjusted by changing the concentration of GO dispersion. The top-right and bottom-right SEM images of Fig. 2c show the GO foam before and after compression. It can be observed that the internal structure of the GO foam is fluffy and porous without compression. Most of the space is filled with air, and the average diameter of the hole structure is roughly on the order of tens of microns. When the GO foam is compressed by external pressure, the air in the foam is squeezed out, resulting in a tight structure, which demonstrates the sensitivity of the GO foam as a pressure sensor. Fig. 2d and e show the Raman spectra of the GO film and GO foam, respectively. According to the Raman spectrum of the GO film, the G peak of GO is at around 1587 $cm^{-1}$, which reflects the symmetry of the graphitic structure, while the D peak of GO is at around 1352 $cm^{-1}$, representing the disorder of the inner sheet of GO. The reason is that the introduction of oxygen-containing functional groups in the oxidation process destroys the original regular electron arrangement structure of graphene. The transformation of $sp^2$ to $sp^3$ causes damage to some C=C bonds and introduces a large number of defects, which are expressed in the enhancement of the D peak and the broadening of the G peak in the Raman spectrum. From the Raman spectrum of the GO foam, it is demonstrated that the Raman peak of the prepared GO foam is very close to that of the GO film, except that the GO foam has more bimodal burrs which may be due to the numerous hole structures in the GO foam. The structural composition of the sandwich-structured pressure sensor is characterized in Fig. 2f. The thin GO/PI composite bilayer film is used as the substrate, and the patterned electrode based on conductive tape is fabricated on the substrate, which is covered by the GO foam. On top of the GO foam is the other layer of pattered electrodes based on conductive tape.

## Movement performance

The soft gripper based on the GO/PI composite bilayer film has excellent photothermal response performance. IR excitation with a power density of 0.2242 W $cm^{-2}$ is applied to the soft gripper, the emitted infrared wavelength of which is 780–3000 nm to obtain the bending movement of the soft gripper. The movement process and the corresponding temperature distribution in relation to time are depicted in Fig. 3a. Initially, the gripper is in a straight state. When the IR is turned on, the

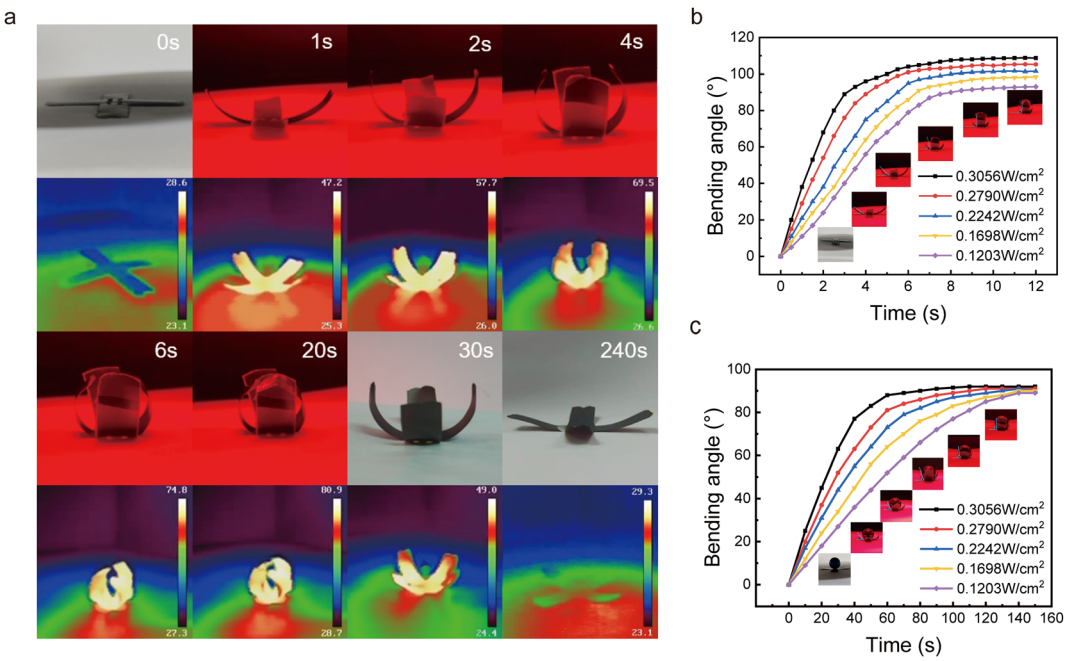


Fig. 3 Mechanical properties of the gripper. (a) Bending movement and temperature distribution of the gripper under the irradiation of IR. (b) Time-dependent bending angle of the unloaded gripper under the irradiation of IR with different power densities; (c) time-dependent bending angle of the gripper grasping the ball under the irradiation of IR with different power densities.

fingers of the gripper quickly bend towards the side of the GO film. After 6 seconds, the fingers of the gripper bend upward about 90° from the straight state. Afterward, with the continuous irradiation of IR, the fingers of the gripper still bend to a certain angle at a slower speed compared with the beginning of the IR irradiation, and remain stable for 20 seconds. When the IR is removed, the fingers of the gripper gradually recover from the curved state to the straight state with time. The bending angle of the fingers changes rapidly at first, and as they gradually approach the straight state, the change in the bending angle decreases. After 240 seconds, the fingers of the gripper return to the straight state, according to the first line and the third line in Fig. 3a.

In order to clarify the photothermal driving principle of the gripper, the temperature change of the gripper under the irradiation of IR is detected by a visual thermometric thermal imager, as displayed in the second and the fourth lines of Fig. 3a. It is implicated that under the irradiation of IR, the temperature of the gripper is much higher than that of the surrounding environment. Because the IR is irradiated vertically from the top of the gripper, heat is evenly distributed across the gripper. When the IR is removed, the temperature of the gripper gradually decreases with time, and the temperature of the fingers decreases faster than that of other parts of the gripper. Finally, the temperature of the gripper returns to the initial temperature, corresponding to the straight state of the gripper. By analysing the temperature distribution of the gripper corresponding to the bending state, it can be confirmed that the bending movement of the gripper is induced by light-induced heat.

In order to study the influence of IR power density on the bending movement of the soft gripper, the gripper is placed under IR with 5 different power densities. The bending angle in Fig. 3b and c is defined in Fig. S1.† According to Fig. 3b, under the irradiation of IR with different power densities, the maximum bending angle and the time taken to reach that are different with the gripper unloaded. At the straight state, the gripper bends quickly under the irradiation of IR, which is manifested as a large slope of the curve in the initial stage. With the continuous irradiation of IR, the fingers of the gripper still bend at a slower speed compared to the initial stage. After stabilization, the gripper reaches the maximum bending angle. In addition, the higher power density of the IR costs less time to reach the same bending angle, leading to a faster response speed. Therefore, under the irradiation of IR with a higher power density, the gripper reaches the maximum bending angle state faster, and then enters a stable state. 15 cycles of repetition experiments are conducted to verify the reliability of the gripper motion. The results are shown in Fig. S4.†

Further study on the response performance when the gripper grasps the object is conducted. Fig. 3c shows the variation of the bending angle with time when the gripper grasps the ball under the IR irradiation of 5 different power densities. Under the irradiation of IR, the response performance of the gripper grasping the ball is different from that of unloaded, especially the maximum bending angle and the time cost under the same power density. For example, under the IR irradiation of 0.3056 W $cm^{-2}$ power density, the time to reach the maximum bending angle is about 6 seconds with the gripper unloaded, while it becomes 105 seconds with the ball grasped. In addition, the maximum bending angle that the gripper finally achieves under different power densities also becomes smaller than the unloaded state, which tends to be near the same angle of 90°. Higher power density induces a faster response speed of the gripper, which costs a shorter time to reach the maximum bending angle and enter the stable state. The longer time to reach the maximum bending angle when grasping the ball is due to that the ball blocks the IR irradiation, which results in a slow rise of temperature in the part that plays a crucial role in the entire grasping movement. Thus, it is necessary for a long time to gradually increase the temperature of obscured parts through heat transfer in order to achieve the maximum bending state. As for the irradiation of IR with different power densities when grasping the ball, the maximum bending angle of the grasping hand tends to be near the same angle, which just meets the requirements of holding the ball.

### Pressure sensor

As shown in Fig. 4, IR excitation with different power densities is applied to the gripper based on the GO/PI bilayer film for the pressure tactile sensing test, and the data are transmitted by the LC circuit. A small ball is placed in the central area of the soft gripper, and a total of 8 IR power densities in the range of 0.0001–0.3056 W $cm^{-2}$ are sequentially applied. Fig. 4a shows the test results of the reflection coefficient $S_{11}$ of the gripper. The LC passive wireless sensor system is in the initial state with no external IR excitation, where the resonant frequency and the $S_{11}$ value at the resonant frequency are 873.2 MHz and −9.89 dB. When the IR excitation is applied to the gripper, the gripper begins to bend and grasp the small ball, which compresses the GO foam dielectric layer of the capacitive pressure sensor and increases the capacitance value, resulting in the left shift of resonant frequency. As depicted in Fig. 4a, the resonant frequency changes insignificantly under the IR power density of 0.0001 W $cm^{-2}$, while it becomes obvious enough to obtain a shift of 2.0 MHz under the IR power density of 0.0264 W $cm^{-2}$. When the power density reaches 0.3056 W $cm^{-2}$, the resonant frequency of the system is 851.6 MHz, and the corresponding $S_{11}$ value is −5.34 dB. The resonant frequency of the gripper pressure sensor continuously shifts to the left with the increase of the power density of IR excitation. In addition, the decrease of the absolute value of $S_{11}$ at the resonant frequency is due to the increasing capacitance reducing the quality factor of the LC circuit, which however has no effect on the detection of the pressure that depended on the resonant frequency shift.

Fig. 4b shows the resonant frequency shift of the gripper's pressure sensor with pressure, the scatters of which correspond to the measurement IR power density in Fig. 4a. The sensitivity of the pressure sensor is 52.7 kHz $mN^{-1}$. Under the irradiation of IR, the shift in the resonant frequency of the gripper in this paper can reach 22.1 MHz. At the same time, in order to test whether the pressure sensing of the gripper is repeatable, the gripper is tested 15 times under the IR with 8 power densities,

 

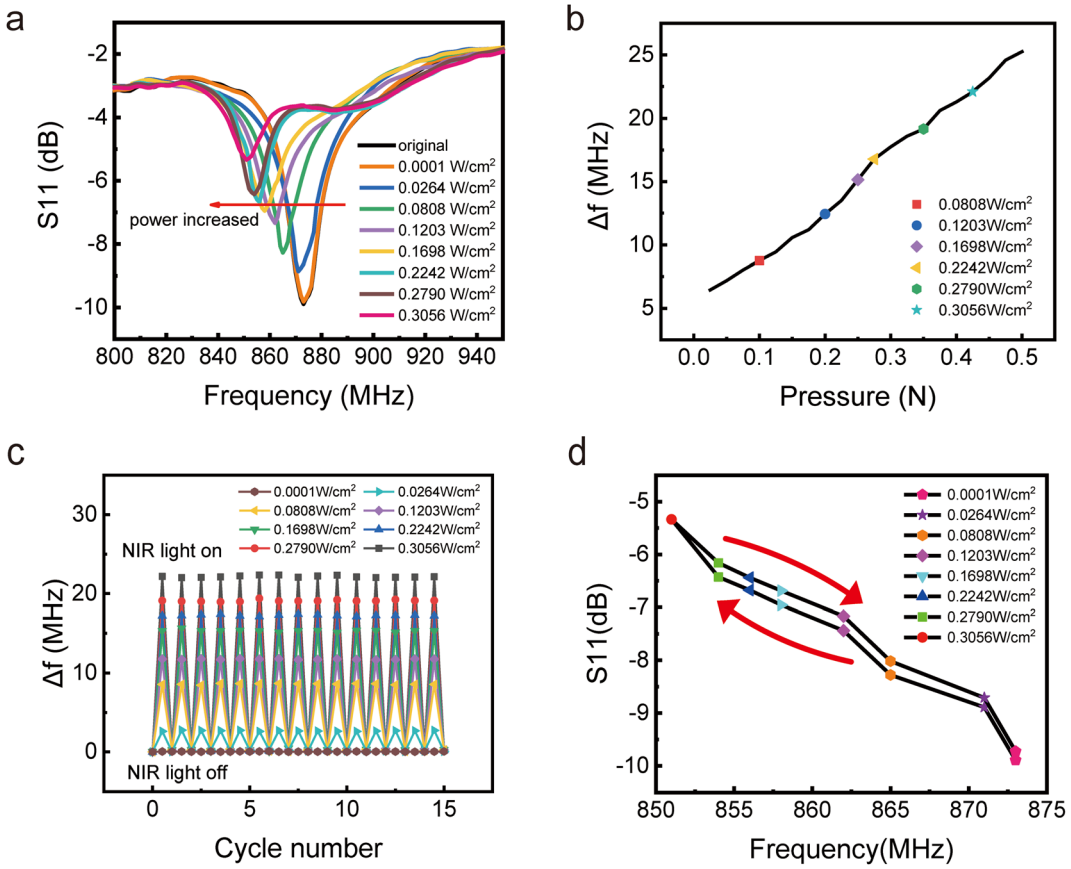


Fig. 4 Pressure sensing test of the gripper. (a) Pressure sensing resonant frequency and $S_{11}$ parameters of the gripper; (b) resonant frequency shift of the pressure sensor on the gripper in relation to pressure, scatters: measurement of power density in (a); (c) gripper pressure sensing repeatability test; (d) hysteresis measurement of a gripper pressure sensor.

as recorded in Fig. 4c. The shift of resonant frequency remains stable after the test, which indicates that the driving performance and the pressure sensing performance show high repeatability and reliability. In addition, hysteresis as an important index to evaluate the stability of the sensor is measured. The power density of the IR continuously increases to the maximum, and then gradually recovers to the initial state. The corresponding resonant frequency and $S_{11}$ value are recorded in Fig. 4d. It can be observed that over a cycle of measurements, only the value of $S_{11}$ shows hysteresis, while the resonant frequency remained stable, which reflects the accuracy response to the pressure, indicating that the pressure sensor of the gripper exhibits high stability. Furthermore, we tested the response of the pressure sensor without objects. As shown in Note S6 and Fig. S8a,† the gripper has only a small shift that can be ignored.

### Material sensor

By imitating the characteristics that human hands can recognize materials according to roughness, the ability to distinguish materials is realized on the gripper. Balls of different diameters and materials are placed in the central area of the grasping hand, and IR with different power densities is applied to observe the shift of the resonant frequency. The material and specific dimensions of the balls are shown in Table S1.† The relative permittivity of the balls of different materials is shown in Table S2.†

Under the irradiation of 8 different IR power densities, the material distinction performance of the gripper is tested. Fig. 5a shows the $S_{11}$ test result of the material sensor of the gripper with a 16 mm wood ball. When no external IR excitation is applied on the gripper, the LC circuit is in the initial state with 2.15 GHz of resonant frequency and −22.84 dB of the corresponding $S_{11}$ value. After applying IR excitation to the gripper, the gripper bends and grasps the ball. The contact area between a pair of interdigital electrodes on the fingers and the ball gradually increases. As the contact grows closer, the relative dielectric constant between the interdigital electrodes gradually approaches that of the ball from the initial value, which changes the interdigital capacitance value and leads to the shift of the resonant frequency. As the IR power density increases, the resonant frequency shifts to the left. When the power density is 0.3056 W cm$^{-2}$, the resonant frequency is 851.6 MHz, and the corresponding $S_{11}$ value becomes −18.94 dB. Under the same IR excitation, the resonant frequency shift of the material sensor is lower than that of the pressure sensing, which is due to that the change in relative permittivity has a relatively small effect on the capacitance value of the interdigitated electrodes. After

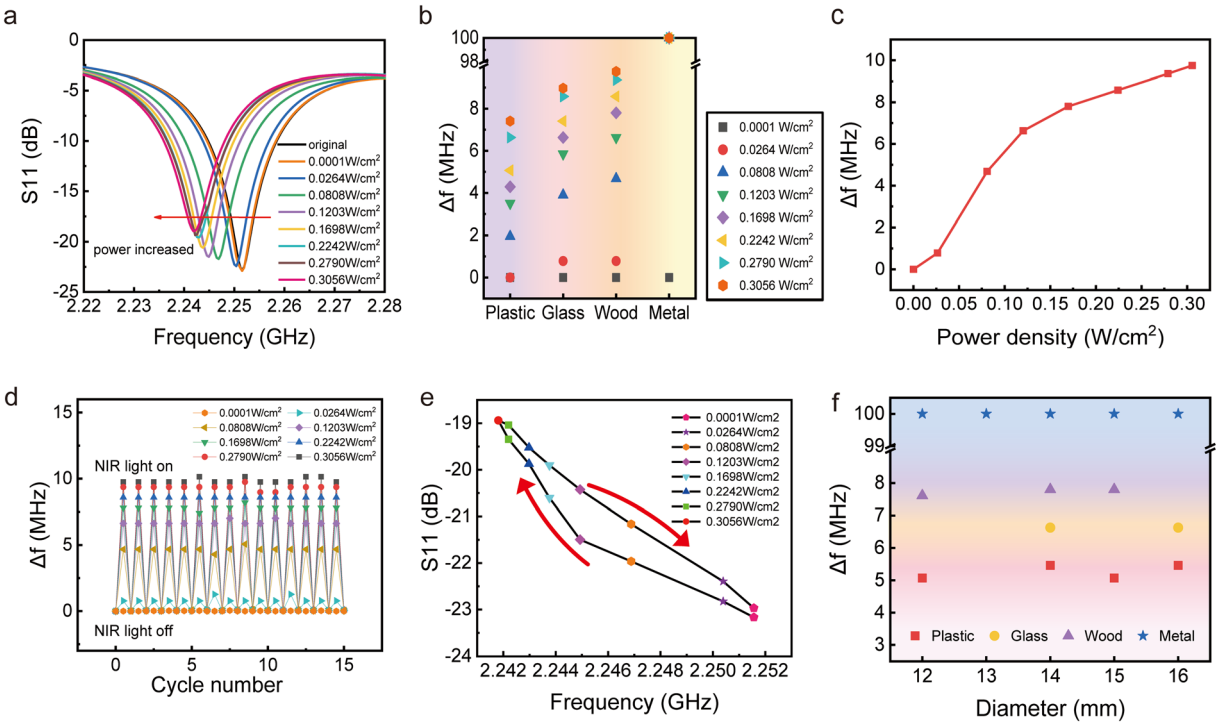


Fig. 5 Material distinction sensing test. (a) $S_{11}$ parameter test results of the gripper's material sensor; (b) material distinction performance of a gripper under different power densities; (c) resonant frequency shift for material distinction of the gripper with different power densities; (d) gripper material distinguishing repeatability test; (e) hysteresis measurement of material sensors; (f) influence of the ball diameter on material distinction.

a significant shift, the change in frequency gradually diminishes with the increase of the IR power density, the reason for which is that the contact area between the interdigitated electrodes on grasping fingers and the ball does not change obviously, resulting in a small change in capacitance.

In order to test the performance of the gripper to distinguish materials, plastic, glass, wood, and metal balls with a diameter of 16 mm are placed under the IR excitation of 8 power densities to monitor the performance of the gripper's material sensor. As captured in Fig. 5b, the gripper begins to distinguish materials after the power density grows to a certain level. Under the same power density, the shift of resonant frequencies corresponding to grasping the plastic, glass, and wood balls increases in turn. However, the resonant peak suddenly disappears once the gripper comes into contact with the metal ball, which is due to that the conducting metal generates a short between the interdigital electrodes. On the other hand, it is observed that with the increase of power density, the resonant frequency shift corresponding to each material gradually increases, inducing that the shift of resonant frequencies corresponding to balls of different materials at higher power density and lower power density appears to overlap. For example, the resonant frequency shift of wood under 0.1203 W cm$^{-2}$ power density is 6.63 MHz, which is the same as the resonant frequency shift of plastic under 0.2790 W cm$^{-2}$ power density. To avoid a miscalculation, the material sensor of the gripper should be tested under the same IR excitation.

Fig. 5c shows the relationship between the power density and the resonant frequency of the wood ball, which reflects the influence of the power density on the gripper's ability to distinguish materials. After reaching the minimum threshold power density for testing, the resonant frequency changes greatly with the increase of the power density. With the further increase of the power density, the resonant frequency begins to change slowly, and the maximum shift of resonant frequency is 9.75 MHz. 15 repeated tests are carried out on the gripper with the wood ball, as demonstrated in Fig. 5d. Both the driving of the gripper robot and the function of distinguishing materials have certain stability, indicating the excellent repeatability and reliability of the gripper.

Fig. 5e depicts the hysteresis curve of the gripper's distinction of wood material. It is indicated that although the $S_{11}$ value at the resonant frequency of the material sensor under the same IR power density is different during the cycle test, the resonant frequency has little change. The maximum hysteresis value appears under the IR excitation with a power density of 0.2790 W cm$^{-2}$, which is only 0.94%. The material sensor of the gripper has good stability.

IR excitation with a power density of 0.1698 W cm$^{-2}$ is applied to the balls with different diameters and materials, to study the effect of the size of the ball on the material distinguishing function as shown in Fig. 5f. It is observed that the size of the diameter has little effect on the material distinction, which will not generate misjudgement. It can be proved that the

gripper has high tolerance for grasping objects. In addition, the material sensor without objects is tested and the result is recorded in Fig. S8b.† A reverse shift of resonant frequency can be observed, which could be predicted by the structure, and does not affect the performance of the sensor, as analysed in Note S6.†

### Gripper system

Finally, an integrated gripper system is set up to imitate the grasping ability of human hands. Fig. 6a shows the process flow for the gripper system from acquisition to analysis. The reading system of the gripper is connected to a PC through a network analyser to analyse the signal. After being determined by a program, the material and grasping force of the target object are displayed in real-time. Four types of balls are tested to demonstrate the gripper system, as shown in Fig. 6b and ESI Movie.† By acquiring and processing the signal data in real-time, the grasping force of the gripper and the material of the object are displayed intelligently. The integrated gripper system can accurately display tactile sensing information such as the grasping pressure of the gripper and the material of the grasped object under the IR excitation, facilitating the gripper's integrated application.

We compared this with previous grippers on the following aspects: material, whether it is flexible, whether it has sensing capabilities, and whether the sensing information can be transmitted wirelessly, as shown in Table 1. We have also compared the studies on tactile sensors to date in Note S7 and Table S3,† which shows that there is no solution that is fully applicable to soft grippers. As a result, we first successfully integrated wireless sensors into a soft gripper, giving the

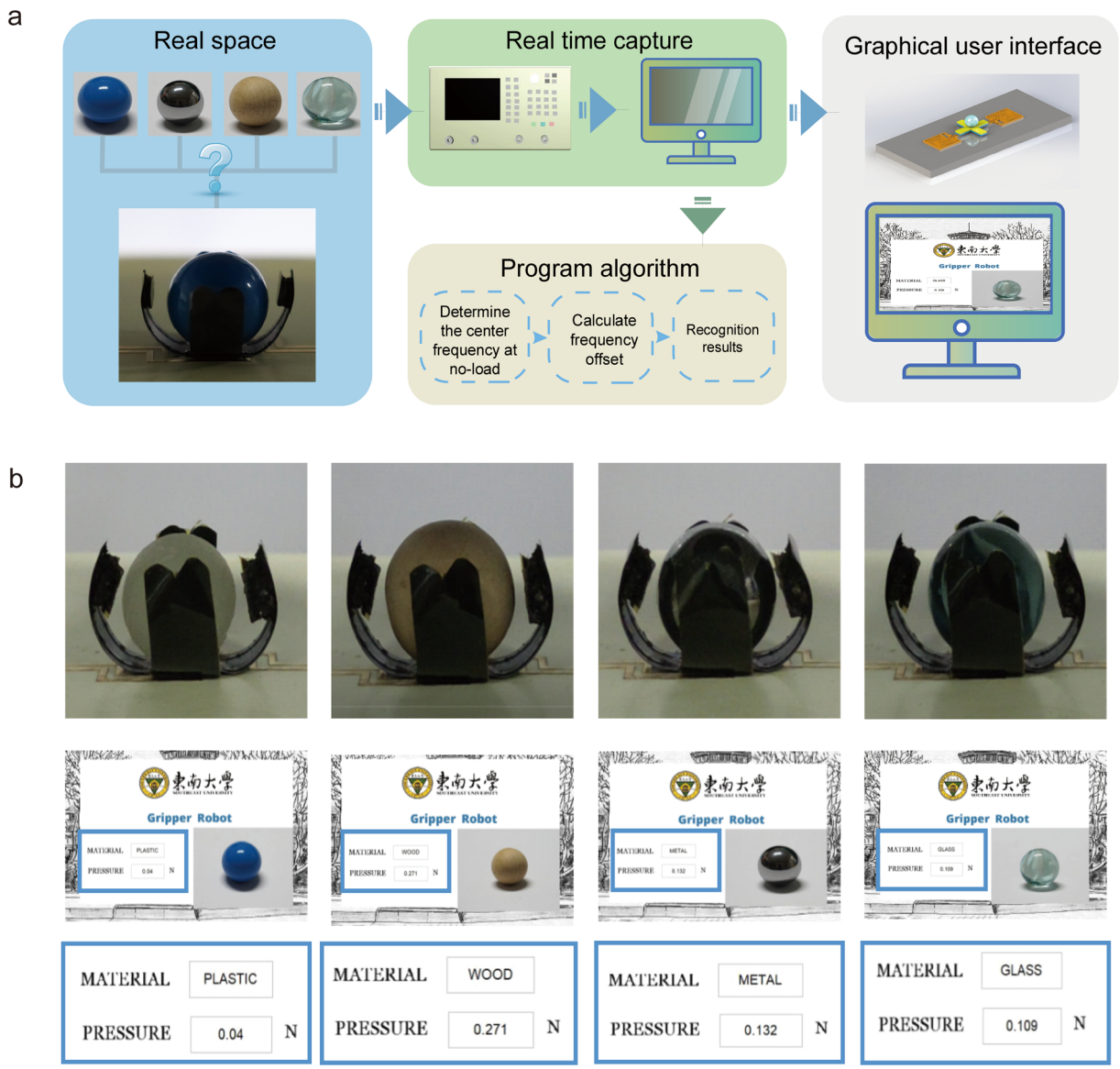


Fig. 6 Imitating human grasping test of the gripper. Grasping recognition test of the gripper. (a) Process flow of the integrated gripper system. (b) Imitating human grasping test results of plastic, wood, metal and glass balls.

Table 1 Comparison of this with the previous grippers

| | Materials | Flexible or rigid | Sensors | Wireless |
|---|---|---|---|---|
| 26 | Hydrogel | Flexible | No | — |
| 10 | GO/BOPP | Flexible | No | — |
| 30 | GO/rGO | Flexible | No | — |
| 34 | SRGO/PI | Flexible | No | — |
| 15 | Hydrogel | Flexible | No | — |
| 32 | PEDOT–PDMS | Flexible | No | — |
| 31 | GO–PDMS | Flexible | No | — |
| 36 | $Ti_3C_2T_x$/polymer | Flexible | No | — |
| 35 | — | Rigid | Thermal-conductivity<br>Pressure<br>Temperature | No |
| 37 | rGO–BOPP | Flexible | Strain | No |
| This work | GO/PI | Flexible | Pressure<br>Material | Yes |

gripper the ability to feel and transmit information without being tied to an electrical connection, which makes the application of soft grippers more promising.

## Experimental

### Preparation of the GO film

First, the GO dispersion (purchased from XFNANO) was added to a filter bottle with filter paper and fixed, and then the vacuum pump was turned on for vacuum filtration to remove the moisture in the dispersion. The GO film was obtained on the filter paper. The still moist GO film was dried in a constant temperature drying oven at 40 °C, and the dried GO film was dark brown and had a smooth and bright surface.

### Preparation of GO foam

First, 100 mg of single-layer GO powder was dispersed in 10 ml of deionized water, and ultrasonically treated for about 30 minutes to obtain a high concentration of 10 mg $ml^{-1}$ GO dispersion as the precursor. The dispersion was yellow brown and viscous, and then the GO dispersion droplet was applied to the GO film side of the GO/PI composite bilayer to prepare a high-concentration GO dispersion; then the temperature of the freeze dryer was lowered to −50 °C and stabilized for 1 hour. Then, the sample was put into a cold trap and freezed for about 1 hour to ensure that the GO dispersion was completely frozen into ice. After the GO dispersion was completely frozen, the compressor was turned off to stop cooling, and the freeze dryer was evacuated to start vacuum drying to directly sublime the water in the frozen GO dispersion, resulting in graphene oxide foam. This process took 9 to 12 hours, and during the drying process, it was found that the ambient air pressure gradually decreased and the ambient temperature increased slowly.

## Conclusions

In conclusion, we have developed a GO/PI composite bilayer film-based gripper that can respond to light, which combines a small soft gripper with tactile sensors and adopts LC passive wireless transmission. The LC circuit transmits tactile information acquired by sensors on the gripper to obtain the grasping pressure and the material of the grasped object, so that it can imitate the motion of human hands grasping objects. Finally, by connecting the gripper system to the processor, it can be effortless to realize the intelligent display of information, which gives the gripper a wide range of applications.

## Author contributions

L. H.: conceptualization, writing – review & editing, supervision, project administration, funding acquisition; R. W.: writing – original draft, visualization, investigation; Y. P. D.: validation, software; X. Z.: investigation, methodology, validation; C. G. W.: methodology, investigation; X. G. Z.: supervision, formal analysis.

## Conflicts of interest

There are no conflicts to declare.

## Acknowledgements

The authors would like to acknowledge the support by the National Natural Science Foundation of China under Grant 62174027.

## Notes and references

1 L. Hines, K. Petersen, G. Z. Lum and M. Sitti, *Adv. Mater.*, 2017, **29**, 1603483.
2 M. Ilami, H. Bagheri, R. Ahmed, E. O. Skowronek and H. Marvi, *Adv. Mater.*, 2021, **33**, 2003139.
3 J. Shintake, V. Cacucciolo, D. Floreano and H. Shea, *Adv. Mater.*, 2018, **30**, 1707035.
4 L. Zhou, L. L. Ren, Y. Chen, S. C. Niu, Z. W. Han and L. Q. Ren, *Adv. Sci.*, 2021, **8**, 2002017.

5 G. F. Cai, J. H. Ciou, Y. Z. Liu, Y. Jiang and P. S. Lee, *Sci. Adv.*, 2019, **5**, eaaw7956.
6 Y. Hu, K. Qi, L. F. Chang, J. Q. Liu, L. L. Yang, M. J. Huang, G. Wu, P. Lu, W. Chen and Y. C. Wu, *J. Mater. Chem. C*, 2019, **7**, 6879–6888.
7 J. M. Liang, Y. C. A. Wu, J. K. Yim, H. M. Chen, Z. C. Miao, H. X. Liu, Y. Liu, Y. X. Liu, D. K. Wang, W. Y. Qiu, Z. C. Shao, M. Zhang, X. H. Wang, J. W. Zhong and L. W. Lin, *Sci. Robot.*, 2021, **6**, eabe7906.
8 W. Tang, C. Zhang, Y. D. Zhong, P. A. Zhu, Y. Hu, Z. D. Jiao, X. F. Wei, G. Lu, J. R. Wang, Y. W. Liang, Y. Q. Lin, W. Wang, H. Y. Yang and J. Zou, *Nat. Commun.*, 2021, **12**, eabe7906.
9 O. M. Wani, H. Zeng and A. Priimagi, *Nat. Commun.*, 2017, **8**, 2247.
10 L. Z. Chen, M. C. Weng, P. D. Zhou, L. L. Zhang, Z. G. Huang and W. Zhang, *Nanoscale*, 2017, **9**, 9825–9833.
11 D. D. Han, Y. L. Zhang, H. B. Jiang, H. Xia, J. Feng, Q. D. Chen, H. L. Xu and H. B. Sun, *Adv. Mater.*, 2015, **27**, 332–338.
12 D. D. Han, Y. L. Zhang, Y. Liu, Y. Q. Liu, H. B. Jiang, B. Han, X. Y. Fu, H. Ding, H. L. Xu and H. B. Sun, *Adv. Funct. Mater.*, 2015, **25**, 4548–4557.
13 Y. Jiang, C. G. Hu, H. H. Cheng, C. X. Li, T. Xu, Y. Zhao, H. B. Shao and L. T. Qu, *ACS Nano*, 2016, **10**, 4735–4741.
14 Q. Li and C. Liu, *Nanotechnology*, 2020, **31**, 085501.
15 S. R. Goudu, I. C. Yasa, X. Hu, H. Ceylan, W. Hu and M. Sitti, *Adv. Funct. Mater.*, 2020, **30**, 2004975.
16 M. Behl, K. Kratz, J. Zotzmann, U. Noechel and A. Lendlein, *Adv. Mater.*, 2013, **25**, 4466–4469.
17 C. Huang, J.-a. Lv, X. Tian, Y. Wang, Y. Yu and J. Liu, *Sci. Rep.*, 2015, **5**, 17414.
18 B. Gorissen, W. Vincentie, F. Al-Bender, D. Reynaerts and M. De Volder, *J. Micromech. Microeng.*, 2013, **23**, 045012.
19 R. Niiyama, X. Sun, C. Sung, B. An, D. Rus and S. Kim, *Soft Robot.*, 2015, **2**, 59–70.
20 H. Zhao, K. O'Brien, S. Li and R. F. Shepherd, *Sci. Robot.*, 2016, **1**, eaai7529.
21 Q. W. Li and C. H. Liu, *Nanotechnology*, 2020, **31**, 085501.
22 Y. Y. Xiao, Z. C. Jiang, X. Tong and Y. Zhao, *Adv. Mater.*, 2019, **31**, 1903452.
23 C. Yang, Z. A. Liu, C. Chen, K. Shi, L. Zhang, X. J. Ju, W. Wang, R. Xie and L. Y. Chu, *ACS Appl. Mater. Interfaces*, 2017, **9**, 15758–15767.
24 S. I. Rich, R. J. Wood and C. Majidi, *Nat. Electron.*, 2018, **1**, 102–112.
25 B. Han, Y.-L. Zhang, L. Zhu, Y. Li, Z.-C. Ma, Y.-Q. Liu, X.-L. Zhang, X.-W. Cao, Q.-D. Chen, C.-W. Qiu and H.-B. Sun, *Adv. Mater.*, 2019, **31**, e1806386.
26 C. Ma, W. Lu, X. Yang, J. He, X. Le, L. Wang, J. Zhang, M. J. Serpe, Y. Huang and T. Chen, *Adv. Funct. Mater.*, 2018, **28**, 1704568.
27 D. Martella, S. Nocentini, D. Nuzhdin, C. Parmeggiani and D. S. Wiersma, *Adv. Mater.*, 2017, **29**, 1704047.
28 Z. Chen, R. Cao, S. J. Ye, Y. H. Ge, Y. F. Tu and X. M. Yang, *Sens. Actuators, B*, 2018, **255**, 2971–2978.
29 Y. Dong, J. Wang, X. K. Guo, S. S. Yang, M. O. Ozen, P. Chen, X. Liu, W. Du, F. Xiao, U. Demirci and B. F. Liu, *Nat. Commun.*, 2019, **10**, 4087.
30 D. D. Han, Y. Q. Liu, J. N. Ma, J. W. Mao, Z. D. Chen, Y. L. Zhang and H. B. Sun, *Adv. Mater. Technol.*, 2018, **3**, 1800258.
31 Leeladhar and J. P. Singh, *Smart Mater. Struct.*, 2020, **29**, 075022.
32 H. Lim, T. Park, J. Na, C. Park, B. Kim and E. Kim, *NPG Asia Mater.*, 2017, **9**, e399.
33 X. D. Wang, N. D. Jiao, S. Tung and L. Q. Liu, *ACS Appl. Mater. Interfaces*, 2019, **11**, 30290–30299.
34 L. L. Yang, K. Qi, L. F. Chang, A. F. Xu, Y. Hu, H. Zhai and P. Lu, *J. Mater. Chem. B*, 2018, **6**, 32254532.
35 G. Li, S. Liu, L. Wang and R. Zhu, *Sci. Robot.*, 2020, **5**, eabc8134.
36 K. H. Yang, C. C. Fu, C. W. Li, Y. J. Ye, M. Ding, J. H. Zhou, Y. Bai, F. L. Jiao, J. Ma, Q. H. Guo and M. C. Weng, *Sens. Actuators, A*, 2022, **341**, 113553.
37 L. Chen, M. Weng, P. Zhou, F. Huang, C. Liu, S. Fan and W. Zhang, *Adv. Funct. Mater.*, 2019, **29**, 1806057.